Astronomy
&
Astrophysics

The nature of the late achromatic bump in GRB 120326A

A. Melandri[1], F. J. Virgili[2], C. Guidorzi[3], M. G. Bernardini[1], S. Kobayashi[2], C. G. Mundell[2], A. Gomboc[4],
B. Dintinjana[5,4], V.-P. Hentunen[6], J. Japelj[4], D. Kopač[4,2], D. Kuroda[7], A. N. Morgan[8], I. A. Steele[2], U. Quadri[9],
G. Arici[10], D. Arnold[2], R. Girelli[9], H. Hanayama[11], N. Kawai[12], H. Mikuž[5,4], M. Nissinen[6], T. Salmi[6], R. J. Smith[2],
L. Strabla[9], M. Tonincelli[10], and A. Quadri[9]

1 INAF – Osservatorio Astronomico Brera, via E. Bianchi 46, 23807 Merate (LC), Italy
  e-mail: andrea.melandri@brera.inaf.it
2 ARI – Liverpool John Moores University, IC2 Liverpool Science Park, 146 Brownlow Hill, Liverpool, L3 5RF, UK
3 Dipartimento di Fisica e Scienza della Terra, via Saragat 1, 44122 Ferrara, Italy
4 Faculty of Mathematics and Physics, University of Ljubljana, Jadranska 19, 1000 Ljubljana, Slovenia
5 Črni Vrh Observatory, Predgriže 29A, 5274 Črni Vrh nad Idrijo, Slovenia
6 Taurus Hill Observatory, Härkämäentie 88, 79480 Kangaslampi, Finland
7 Okayama Astrophysical Observatory – NAOJ, 3037-5 Honjo, Kamogata, Asakuchi, 719-0232 Okayama, Japan
8 Department of Astronomy, University of California, Berkeley, CA 94720-3411, USA
9 Osservatorio Astronomico Bassano Bresciano, via San Michele 4, 25020 Bassano Bresciano (BS), Italy
10 Osservatorio Astronomico di Cima Rest, via Rest, 25080 Magasa (BS), Italy
11 Ishigakijima Astronomical Observatory – NAOJ, 1024-1, Arakawa, Ishigaki, 907-0024 Okinawa, Japan
12 Department of Physics, Tokyo Institute of Technology, 2-12-1 Ookayama, Meguro-ku, 152-8551 Tokyo, Japan

ABSTRACT

The long *Swift* gamma-ray burst GRB 120326A at redshift $z = 1.798$ exhibited a multi-band light-curve with a striking feature: a late-time, long-lasting achromatic rebrightening that is rarely seen in such events. Peaking in optical and X-ray bands ∼35 ks (∼12.5 ks in the GRB rest frame) after the 70 s GRB prompt burst, the feature brightened nearly two orders of magnitude above the underlying optical power-law decay. By modelling the multi-wavelength light-curves, we investigated possible causes of the rebrightening in the context of the standard fireball model. We excluded a range of scenarios for the origin of this feature: reverse-shock flash, late-time forward-shock peak caused by the passage of the brightest synchrotron frequency through the optical band, late central engine optical or X-ray flares, interaction between the expanding blast wave and a density enhancement in the circumburst medium, and gravitational microlensing. Instead we conclude that the achromatic rebrightening may be caused by a refreshed forward shock or a geometrical effect. In addition, we identify an additional component after the end of the prompt emission, which shapes the observed X-ray and optical light-curves differently, and which rules out a single overall emission component to explain the observed early-time emission.

Key words. gamma-ray burst: general – gamma-ray burst: individual: GRB 120326A

1. Introduction

Gamma-ray bursts (GRBs) are brief and intense pulses of γ-rays (prompt emission) followed by long-lasting afterglow emission that can span the entire electromagnetic spectrum from X-rays to radio bands. Since the advent of the *Swift* satellite (Gehrels et al. 2004) X-ray afterglows have unarguably been the most frequently sampled for most GRBs, from very early times until days or weeks after the burst event. In the context of the standard fireball model, this led to the definition of a canonical light-curve in the X-ray band (Nousek et al. 2006). This definition comprises: 1) an initial steep decay (possibly reminiscent of the high-latitude prompt emission) lasting until ∼10^2 s; 2) a possible shallow (or rising) phase (called plateau) between ∼10^2–10^4 s that might be due to prolonged central engine activity, energy injection into the forward shock, or variation of microphysical parameters; 3) a normal phase up to ∼10^5 s that shows the decaying afterglow emission of the forward-shock interacting with the external medium; 4) a late phase with a steeper decay, that is not always observed, consistent with a jet break. In up to 50% of

GRBs, flare activity caused by internal shocks is seen superimposed on the first two phases (Zhang et al. 2006; Burrows et al. 2007).

At longer wavelengths, the behaviour of the light-curves may not always follow that observed in the X-rays. If the same light-curve features are present contemporaneously in different bands, the behaviour is described as achromatic and the radiation is interpreted as having been produced by a single emission mechanism, or alternatively, the achromatic behaviour is caused by geometric effects, for example late-time steepening of the light-curves hours to days after the GRB, caused by a jet break.

In contrast, early-time emission is often chromatic because the typical synchrotron frequencies pass through the observing bands. In addition, multiple emission components from different locations in the relativistic outflow may be temporally superimposed on the observed light-curve. The key components of the early afterglow are expected to be emission from the external reverse and forward shocks (Japelj et al. 2014), with the possibility of additional flares or re-brightenings as a result of energy

injection from long-lived central engine activity (Melandri et al. 2009; Virgili et al. 2013), or interaction between the advancing shock and inhomogenities in the circumburst medium (Mundell et al. 2007). In a few GRBs with optical emission observed contemporaneously with the prompt γ-ray emission, rapid variability ($\Delta t/t \lesssim 1$) and steep rise or decay indices indicate an internal dissipation for the origin of the optical emission (Monfardini et al. 2006; Kopač et al. 2013).

Overall, chromaticity is more often seen in GRB afterglow light-curves, with only a minority of bursts clearly showing a similar behaviour in the X-ray and optical bands (Panaitescu et al. 2006; Ghisellini et al. 2009; Melandri et al. 2010, 2014; Nardini et al. 2011a; Guidorzi et al. 2014). With high-quality data, the similarity between the X-ray and optical bands in these bursts is striking (GRB 100901A, Gomboc et al., in prep.; GRB 081028, Margutti et al. 2010), while for others the evidence for achromaticity is only marginal (GRB 071010A, Covino et al. 2008; GRB 091029, Filgas et al. 2012).

Here we present high-quality, panchromatic observations from X-ray to radio bands of GRB 120326A, which exhibits an unusual and pronounced late-time achromatic bump occurring simultaneously in X-ray and optical bands between $10^3 - 10^5$ s in the rest-frame of the burst. We test a wide range of different scenarios to explain the re-brightening: reverse-shock emission, the passage of the typical frequency, the onset of the afterglow, a refreshed shock, a late-time flare, a density enhancement of the ambient medium, a geometrical effect, and gravitational microlensing. Throughout the paper we assume a standard cosmology with $H_0 = 72$ km s^{-1} Mpc^{-1}, $\Omega_m = 0.27$, and $\Omega_\Lambda = 0.73$. The respective temporal and spectral decay indices α and β are defined by $f_\nu(t) \propto t^{-\alpha}\nu^{-\beta}$, and unless stated otherwise, errors are only statistical.

2. Observations

On 2012 March 26 at 01:20:29 UT ($=T_0$), the *Swift*/BAT triggered on the long GRB 120326A (Siegel et al. 2012). The BAT light-curve showed two well-defined precursor peaks (each ~30 s wide) followed by a main Fast Rise Exponential Decay (FRED) peak that returned to the background level after ~20 s. The total duration of the burst was $T_{90} = 69 \pm 8$ s (Barthelmy et al. 2012).

Swift/XRT promptly detected the afterglow emission in the X-ray with good precision within ~1 min after the event, whereas *Swift*/UVOT was not able to detect any credible candidate in the optical bands during its first observations. The optical afterglow was detected a few minutes later from the ground by small (TAROT; Klotz et al. 2012a) and large (Liverpool Telescope; Guidorzi et al. 2012) robotic telescopes, which identified a slowly decaying counterpart.

Spectroscopic observations performed with the 10.4 m GTC telescope ~2 h after the event showed several absorption features at a common redshift of $z = 1.798$ (Tello et al. 2012). This event was also detected by Fermi-GBM and displayed an average γ-ray fluence of ~3.5×10^{-6} erg cm^{-2} in the 10–1000 keV band with a peak energy $E_{\text{peak}} = 46 \pm 4$ keV (Collazzi 2012). The redshift of the burst (corresponding to a luminosity distance of ~1.37×10^4 Mpc) resulted in an isotropic energy estimate of $E_{\gamma,\text{iso}} = (3.45 \pm 0.14) \times 10^{52}$ erg in the rest-frame [1–10 000] keV bandpass.

2.1. Optical and near-infrared data

The optical afterglow reported by Klotz et al. (2012a) was observed by many telescopes in the subsequent days. We acquired

images in the optical bands ($g'Ri'z'$), starting from ~3.5 min after the burst, with the 2 m Liverpool robotic telescope (Guidorzi 2012), the 0.6 m Cichocki robotic telescope at the Črni Vrh Observatory (Dintinjana et al. 2012), the 0.43 m T17 telescope (Hentunen et al. 2012), the 0.32 m robotic telescope at the Bassano-Bresciano Observatory (Quadri et al. 2012a–e), the MITSuME 1.05 m telescope at the Ishigakijima Observatory (Kuroda et al. 2012a,b,c), and the 0.51 m telescope at the Cima Rest Observatory (Tonincelli et al. 2012). Near-infrared data were acquired with the 1.3 m Pairitel telescope in the JHKs-bands (Morgan 2012). A summary of our observations is given in Table 1.

2.2. Radio, mm, and sub-mm data

The afterglow of GRB 120326A was detected by the Sub-Millimeter Array (SMA, Urata et al. 2012, 2014) at the typical frequency of $\nu_{\text{SMA}} = 219$ GHz at a flux density of $f_{\text{SMA}} = 3.1 \pm 0.5$ mJy, by the Combined Array for Research in Millimeter-Wave Astronomy (CARMA, Perley et al. 2012) at $\nu_{\text{CARMA}} = 92.5$ GHz at a flux density of $f_{\text{CARMA}} = 3.2 \pm 0.4$ mJy and by the Expanded Very Large Array (EVLA, Laskar et al. 2012) at $\nu_{\text{EVLA}} = 21.9$ GHz at a flux density of $f_{\text{EVLA}} \sim 1.36$ mJy.

3. Results

We calibrated our optical images with respect to several field stars. In particular, we calibrated SDSS-r' images acquired with LT with respect to the R band to obtain a well sampled R-band light-curve from early to late times. Then we converted the observed optical-NIR magnitudes (Table 1) into flux densities (Fukugita et al. 1995) after taking into account the Galactic extinction ($E_{(B-V)} = 0.05$, $A_B = 0.182$ mag, $A_{g'} = 0.169$ mag, $A_V = 0.134$ mag, $A_R = 0.106$ mag, $A_{i'} = 0.074$ mag, $A_{z'} = 0.063$ mag, $A_J = 0.035$ mag, $A_H = 0.022$ mag, $A_K = 0.015$ mag; Schlafly & Finkbeiner 2011).

3.1. Light-curve

In Fig. 1 (left panel) we report the optical and X-ray light-curves of GRB 120326A. We fit the X-ray and best-sampled optical band (R filter) independently, in the time interval [10–10^6] s, with the same number of components: a single power-law decay (PL) plus smoothly broken-power law (BPL, Beuermann et al. 1999) to reproduce the bump. All the other optical wavelengths agree very well with a rigid shift of the final fitting function for the R band. The results of the fit are reported in Table 2. The peaks in the X-ray and optical bands peak at almost the same time (~0.4 d), suggesting an achromatic bump.

Despite the different behaviour before the peak, there is certainly an additional emission component that enhances the observed flux in the X-ray and optical bands. The early-time power-law decay (α_{PL}) and the rising slopes ($\alpha_{\text{BPL,rise}}$) are clearly inconsistent with a single emitting region for the two bands. The early-time X-ray light-curve exhibits a steep decay ($\alpha \sim 3.7$) that probably arises from the tail-end of the prompt emission, whereas the optical light-curve exhibits a much shallower decay. In contrast, the peak time (t_{peak}) of the bump in the light-curve at $t \sim 4 \times 10^4$ s is consistent within errors for both the optical and X-ray bands (however, we note that the decay in the X-ray is slightly steeper than the decay observed in the optical). However, optical observations performed at later times than our last optical detection showed that the optical light-curve might

Table 1. Optical observations of GRB 120326A.

Δt	$t_{\rm exp}$	Filter	Magnitude	Ref.	Δt	$t_{\rm exp}$	Filter	Magnitude	Ref.
[s]	[s]				[s]	[s]			
3697	393	B	20.23 ± 0.16	(4)	2715	330	R	19.44 ± 0.67	LT-SkyCam
64 440	300	B	19.40 ± 0.10	(5)	3771	60	R	19.40 ± 0.20	(3)
65 520	300	B	19.40 ± 0.10	(5)	5659	120	R	19.42 ± 0.16	T17
21 959	295	V	18.67 ± 0.12	(4)	5822	120	R	19.27 ± 0.21	T17
64 080	300	V	18.7 ± 0.10	(5)	5985	120	R	19.08 ± 0.14	T17
65 160	300	V	18.8 ± 0.10	(5)	6149	120	R	19.02 ± 0.17	T17
1994	480	SDSS-g'	20.77 ± 0.15	(2)	6311	120	R	19.22 ± 0.15	T17
142 799	1200	SDSS-g'	20.58 ± 0.14	MITSuME	6475	120	R	19.10 ± 0.09	T17
146 890	1140	SDSS-g'	20.62 ± 0.15	MITSuME	15 996	60	R	18.40 ± 0.20	(3)
223 766	2280	SDSS-g'	21.01 ± 0.32	MITSuME	27 640	300	R	17.63 ± 0.20	(6)
317 981	8700	SDSS-g'	21.90 ± 0.19	MITSuME	72 987	13 080	R	18.35 ± 0.07	Bassano Obs.
133	60	R	18.20 ± 0.20	(1)	142 799	1200	R	19.41 ± 0.09	MITSuME
216	240	R	18.52 ± 0.18	LT-RINGO2	146 890	1140	R	19.52 ± 0.09	MITSuME
441	60	R	18.77 ± 0.14	Črni Vrh Obs.	166 916	13080	R	19.33 ± 0.15	Bassano Obs.
508	60	R	18.86 ± 0.19	Črni Vrh Obs.	223 766	2280	R	20.00 ± 0.17	MITSuME
552	320	R	18.74 ± 0.18	LT-RINGO2	253 037	13 080	R	20.10 ± 0.31	Bassano Obs.
575	60	R	18.87 ± 0.15	Črni Vrh Obs.	317 981	4320	R	20.66 ± 0.15	MITSuME
642	120	R	19.03 ± 0.19	Črni Vrh Obs.	323 443	4380	R	20.65 ± 0.14	MITSuME
776	120	R	18.86 ± 0.17	Črni Vrh Obs.	505 266	12 000	R	21.52 ± 0.38	Cima Rest Obs.
841	30	SDSS-r'	18.81 ± 0.16	LT-RATCam	1165	120	SDSS-i'	19.06 ± 0.07	LT-RATCam
910	180	R	18.92 ± 0.11	Črni Vrh Obs.	1775	120	SDSS-i'	19.31 ± 0.06	LT-RATCam
915	270	R	18.83 ± 0.38	LT-SkyCam	2793	360	SDSS-i'	19.40 ± 0.07	LT-RATCam
931	30	SDSS-r'	19.00 ± 0.14	LT-RATCam	3089	800	SDSS-i'	19.24 ± 0.15	(2)
1005	120	SDSS-r'	18.95 ± 0.04	LT-RATCam	183 282	4620	I	19.55 ± 0.20	MITSuME
1111	120	R	19.10 ± 0.15	Črni Vrh Obs.	317 982	8700	I	20.24 ± 0.22	MITSuME
1245	120	R	19.37 ± 0.24	Črni Vrh Obs.	1326	120	SDSS-z'	18.79 ± 0.13	LT-RATCam
1380	180	R	19.48 ± 0.18	Črni Vrh Obs.	2075	240	SDSS-z'	18.87 ± 0.10	LT-RATCam
1478	120	SDSS-r'	19.25 ± 0.05	LT-RATCam	3241	360	SDSS-z'	19.05 ± 0.10	LT-RATCam
1495	945	R	19.10 ± 0.20	(1)	120 852	4727	J	17.8 ± 0.4	PAIRITEL
1581	180	R	19.38 ± 0.22	Črni Vrh Obs.	206 964	4048	J	18.9 ± 0.5	PAIRITEL
1610	120	SDSS-r'	19.33 ± 0.06	LT-RATCam	120 852	4727	H	16.3 ± 0.4	PAIRITEL
2076	640	SDSS-r'	19.87 ± 0.15	(2)	206 964	4048	H	17.3 ± 0.5	PAIRITEL
2363	120	SDSS-r'	19.40 ± 0.06	LT-RATCam	120 852	4727	K	16.03 ± 0.25	PAIRITEL
2495	120	SDSS-r'	19.40 ± 0.05	LT-RATCam	206 964	4048	K	16.45 ± 0.25	PAIRITEL
2627	120	SDSS-r'	19.38 ± 0.06	LT-RATCam					

Notes. Columns are the beginning time (Δt), length ($t_{\rm exp}$) of the exposure, optical filter used for the observations, magnitudes (with errors), and reference to the telescope used for each observation. Magnitudes have not been corrected for Galactic absorption along the line of sight ($E_{(B-V)}$ = 0.05, Schlafly & Finkbeiner 2011). References for data taken from GCNs are: (1) Klotz et al. 2012b; (2) La Cluyze et al. 2012; (3) Walker et al. 2012; (4) Kuin et al. 2012; (5) Zhao et al. 2012; (6) Jang et al. 2012.

Table 2. Light-curve fit results.

Band	$\alpha_{\rm PL}$	$\alpha_{\rm BPL,rise}$	$t_{\rm break}$	$t_{\rm peak}$	$\alpha_{\rm BPL,decay}$	$\chi^2_{\rm red}$ (d.o.f.)
			[s]	[s]		
X-ray	3.72 ± 0.08	-0.38 ± 0.05	$(6.2 \pm 0.4) \times 10^4$	$(3.2 \pm 0.3) \times 10^4$	2.52 ± 0.11	1.20 (238)
Optical	0.50 ± 0.05	-1.53 ± 0.18	$(3.7 \pm 0.4) \times 10^4$	$(3.6 \pm 0.5) \times 10^4$	1.77 ± 0.11	0.95 (37)

Notes. We model the X-ray and optical light-curve with a two-component function: an initial power-law (PL) plus a late-time broken power-law (BPL). Here we report the initial power-law decay ($\alpha_{\rm PL}$), the rising ($\alpha_{\rm BPL,rise}$), the break time ($t_{\rm break}$), the peak time ($t_{\rm peak}$), and the decaying index ($\alpha_{\rm BPL,decay}$) of the second component. The last column shows the goodness-of-fit (reduced χ^2) and the corresponding degrees of freedom.

have undergone another break to a steeper value of $\alpha \sim 2.5 \pm 0.2$ (consistent with the X-ray decay), which indicates a possible jet collimation of a few degrees (Urata et al. 2014).

3.2. Spectral energy distribution

We built the rest-frame spectral energy distribution of the optical afterglow at the post-break time $t_{\rm rf}^{\rm SED} = 1$ d, corresponding to $t_{\rm obs} = 2.798$ d. The X-ray data for this time allows us to constrain

the spectral index ($\beta_{\rm opt-X}$) and the circum-burst absorption ($A_{\rm V}$) under the assumption that the X-ray and optical emission arise from the same spectral component. For these purposes we extracted the X-ray spectrum in the observed time interval [0.4, 2.5] $\times 10^5$ s and re-scaled it to the time selected for the analysis ($t_{\rm SED}$) to match the behaviour of the X-ray light-curve.

The data are best described by a single absorbed power-law SMC-model with $\beta_{\rm opt-X} = 0.88 \pm 0.03$ and $A_V^{\rm GRB} = (1.1 \pm 0.3)$ mag (90% c.l.; χ^2/d.o.f. = 31.6/43). From fixing the Galactic
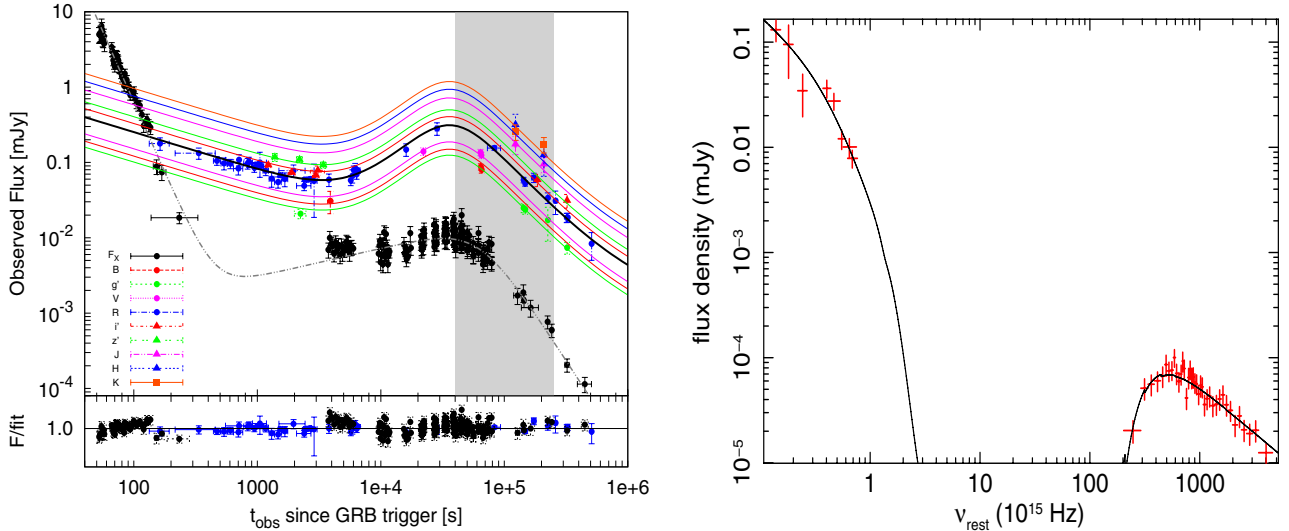
Fig. 1. *Left panel*: panchromatic light-curve of GRB 120326A in the observer frame. In the X-ray band we draw only the function of the final fit (dot-dashed grey line), while for the optical bands we show the final fit for the *R* filter (black solid line) and also the re-scaled fit for each wavelength (coloured lines). The scaling factors for different filters are 0.48, 0.4, 0.6, 1.3, 1.6, 2.3, 3.0, and 3.8 for the *Bg′Vi′z′JHK* bands, respectively. The shaded grey region refers to the time interval during which the XRT spectrum has been extracted. The lower panels show the residuals of the optical and X-ray fits. *Right panel*: spectral energy distribution at the reference time $t_{\rm rf}^{\rm SED} = 1$ d (see main text for details).

column density to $N_{\rm H}^{\rm GAL} = 5 \times 10^{20}$ cm^{-2}, we find an X-ray absorbing column density of $N_{\rm H}^{\rm GRB} = (6.6 \pm 0.3) \times 10^{21}$ cm^{-2}.

4. The nature of the late-time achromatic peak

The light-curve of GRB 120326A displays a smooth prolonged re-brightening at late times, both in the optical and X-ray bands (Fig. 1, left panel). The observed variability might be the result of different processes and can be associated with various forms of late-time energy injection (flare, delayed afterglow onset, re-freshed shock emission), with density inhomogeneities in the circum-burst medium, or some geometrical effect. We now discuss all the possible interpretations of the observed broad peak for GRB 120326A.

4.1. Reverse-shock emission

A bright (optical) peak can be produced by the reverse shock that propagates back into the shocked material. If present, this peak would occur and be visible in the observed light-curve at very early times ($t \leq 10^3$ s), and subsequently the light-curve would display a steep temporal decay index ($t^{-\alpha_{\rm RS}}$ with $\alpha_{RS} \sim 2.0$, Kobayashi & Zhang 2003; Zhang et al. 2003). For GRB 120326A, the rising light-curve after $\sim 5 \times 10^3$ s, with $\alpha_{\rm BPL, rise} \sim -1.5$, was preceded by a relatively shallow phase ($\alpha_{\rm PL} \sim 0.5$). At this time, the optical light-curve had a decay that was too shallow to be associated with a reverse shock, and it is probably related to a different component. Moreover, at very early times no peak is detected and the only peak visible in the optical light-curve occurs at $t_{\rm peak} = (3.6 \pm 0.5) \times 10^4$ s $\sim$ 0.4 d post-burst, too late to be associated with the reverse-shock emission. We note that the post-bump optical decay index ($\alpha_{\rm BPL, decay} \sim 1.8$) is marginally consistent with the expectation for a reverse shock. In summary, this explanation is inconsistent with the observed optical light-curve of GRB 120326A.

4.2. The passage of $\nu_{\rm m}$

The observed peak might be the signature of the passage of the highest synchrotron frequency ($\nu_{\rm m}$) across the optical band. If

this were the case, then the reverse shock would expected to decay as $t^{-0.45}$ (Kobayashi 2000), while the forward shock would rise as $t^{1/2}$ and decay as t^{-1}. In principle, this could better explain the initial part of the optical light-curve and the temporal difference between the lowest flux reached after $\sim 10^3$ s and the optical peak at $\sim 3 \times 10^4$ s. This scenario cannot generate and explain achromatic and coincident peaks at different frequencies, however, as observed for GRB 120326A in the optical and X-ray bands (Fig. 1).

4.3. Onset of the afterglow

The onset of the forward-shock emission has been observed for many bursts, sometimes at very early times (e.g. GRB 060418, Molinari et al. 2007) and a few times also at later times (e.g. GRB 080129, Greiner et al. 2009). The multi-wavelength analysis of the very bright GRB 061007 (Mundell et al. 2007; Rykoff et al. 2009) showed that the onset of the forward shock can sometimes be inferred to take place at $t \lesssim 100$ s after the burst event at the optical frequencies. This implies that the reverse shock must have peaked at a typical frequency that are lower by $\sim \Gamma_0^2$ than the typical frequency of the optical band. If the forward shock peaks in the optical band, for typical values of Γ_0 the reverse shock will peak at the radio frequencies (low-frequency model, see Kobayashi & Zhang 2003 for more details).

As discussed for GRB 061007 (Mundell et al. 2007), and subsequently for GRB 090313 (Melandri et al. 2010) for all the GRBs that display the onset of the optical afterglow it is possible to apply the low-frequency model (Kobayashi & Zhang 2003) to the observed optical data, making predictions for the expected light-curves at radio frequencies. Since for the case we studied here there are few positive detections in the radio-submm band (Urata et al. 2012; Perley et al. 2012; Laskar et al. 2012; Staley et al. 2012), we can therefore apply the model to the radio data to determine whether what is observed in the optical band is the real onset of the forward shock.

In Fig. 2, we compare the confirmed radio detections with the predictions of the low-frequency model in the corresponding radio frequencies. The parameters assumed for the model are $0.1 \leq \epsilon_{\rm e} \leq 0.5$ and $2 \leq p \leq 3$. All the other parameters of the
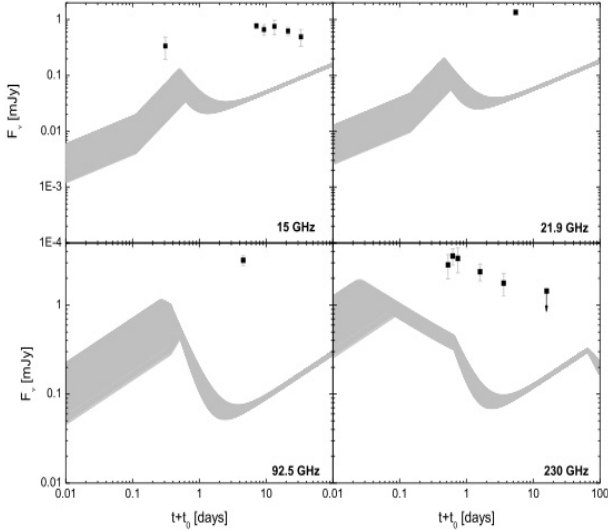
Fig. 2. Light-curve predictions in the radio band in the context of the low-frequency model. We assume the late-time peak as the possible onset of the forward-shock emission. The expected radio light-curve is displayed as a grey region that also reflects the uncertainties on the parameters assumed by the model.

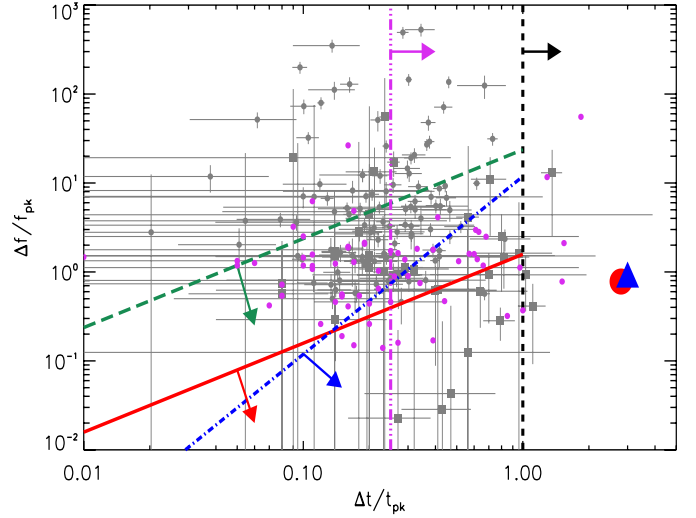**Fig. 3.** Kinematically allowed regions for afterglow variability in the $\Delta f / f_{peak}$ vs. $\Delta t / t_{peak}$ plane. Solid lines with arrows represent the allowed regions for density fluctuations on-axis (blue), density fluctuations off-axis (red), multiple density fluctuations off-axis (green), refreshed shocks (pink) and patchy shell (black; for details see Ioka et al. 2005; Curran et al. 2008; Bernardini et al. 2011). In this plot we show early-time ($t_{peak} \leq 10^3$ s, grey circles; Chincarini et al. 2010) and late-time ($t_{peak} > 10^3$ s, grey squares; Bernardini et al. 2011) X-ray flares together with UV/optical flares detected at 1σ confidence level (magenta circles; Swenson et al. 2013). The X-ray and optical peaks observed for GRB 120326A are shown with a blue triangle and a red circle.

model (Γ_0, E_{iso}, ϵ_B, etc.) were calculated from the available data. The predictions, assuming the late peak as the onset of the forward shock, show that the afterglow is expected to peak in the radio band between 0.01 and 1 days after the burst event depending on the frequency, reaching a highest flux of a few mJy. Although this scenario does not fully describe the radio observations at high frequencies, the radio predictions for $\nu_{radio} \sim 15$ GHz are only a factor of ~3 brighter than the model predictions, as seen in Fig. 2.

It is possible that the real onset of the afterglow occurred much earlier, without being clearly visible in the optical bands. The observed shallow decay for $t \leq 10^3$ s might be the decline of a forward shock that peaked at $t = t' \leq 10^2$ s. In this case, the average $\Gamma_{peak} \sim 187$ and the prediction for the radio emission are even farther removed from the reported radio detection since the grey regions in Fig. 2 would be almost rigidly shifted to the left along the x-axis because the radio light-curve is expected to peak at much earlier times[1]. Again, this scenario is incompatible with the radio afterglow detections reported in literature for GRB 120326A.

4.4. Late-time optical/X-ray flare emission

Emission from flares has been detected for many GRBs, superimposed onto their canonical decays from very early times up to $\gtrsim 10^5$ s after the burst event (Bernardini et al. 2011). The observed afterglow variability can be displayed and compared with the kinematically allowed regions in the plane ($\Delta f / f_{peak}$) vs. ($\Delta t / t_{peak}$), describing the increase of the flux with respect to the underlying continuum versus the temporal variability (Ioka et al. 2005).

As seen in Fig. 3, all the X-ray flares (Chincarini et al. 2010; Bernardini et al. 2011), with the exception of GRB 050724, can be explained in the context of the internal-shocks model, where $\Delta t / t_{peak} < 1$, or single and multiple density fluctuations, if the flux ratio $\Delta f / f_{peak}$ is low. The same conclusions can be drawn in the UV and optical, with the exception of a few more events (see Swenson et al. 2013 for details). However, for GRB 120326A, the observed broad late-time variability in the X-ray and optical bands has $\Delta t / t_{peak} \gg 1$ and therefore cannot be the result of any flare activity. The achromatic bump of GRB 120326A light-curve is more compatible with a possible refreshed shock episode.

4.5. Refreshed shock

Another possibility to explain a late re-brightening in the light-curve is to consider a forward shock that is refreshed by a late-time energy supply (Rees & Mészáros 1998; Kumar & Piran 2000; Sari & Mészáros 2000). At late times, shells emitted with lower or modest Lorentz factor ($\Gamma \sim 10 \div 20$) catch up with faster shells ($\Gamma \geq 100$) that have already been slowed down by the interaction with the external material. These shells inject energy into the afterglow shock and cause a significant re-brightening in the observed light-curve. This scenario has been successfully invoked to explain, for example, the numerous bumps of the optical light-curve of GRB 030329 (Granot et al. 2003).

Under the simplified assumption of only two shells colliding, with $\Gamma_{fast} \geq 10^2$ and $\Gamma_{slow} = \Gamma_0 \sim 10$, it can be shown (see Genet et al. 2006) that the two shells will collide at a time

$$t_{shock} \approx 1.66 \, E_{\gamma,iso,53}^{1/3} \, n^{-1/3} \, \Gamma_{slow,10}^{-8/3} \quad \text{days}, \quad (1)$$

where $E_{\gamma,iso,53}$ is the isotropic energy in units of 10^{53} erg, n is the density of the external medium (assumed to be =1 cm^{-3}

---

[1] The average value for Γ_{peak} is calculated using Eq. (1) from Molinari et al. (2007) with $n = 1$ cm^{-3}. If we assume a radiative efficiency $\eta = 1$, we derive the lower value for the late- (early-) time observed peak of $\Gamma_{peak} = 18$ (≥ 169), while assuming $\eta = 0.2$ we obtain $\Gamma_{peak} = 22$ (≥ 206). These estimates were made assuming a homogeneous circumburst medium; if we assume a wind-like medium ($\rho \sim R^{-2}$), the Lorentz factors for the early and late optical peaks are $\Gamma_{peak}^{wind} \sim 41$ and $\Gamma_{peak}^{wind} \sim 10$, respectively.
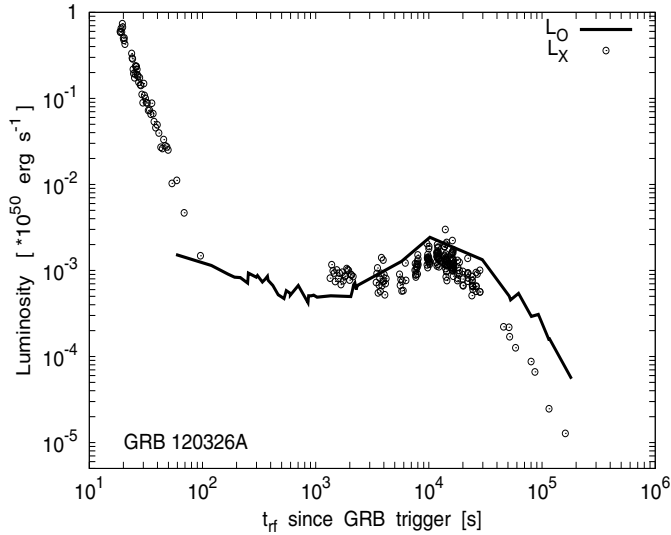
Fig. 4. Rest-frame X-ray (open circles) and optical (solid line) luminosity. At late times the achromatic behaviour of the light-curve is evidence supporting the interpretation of a possible refreshed shock or geometrical effect.

for a uniform medium), and $\Gamma_{\text{slow},10}$ is the Lorentz factor of the slow shell in units of ten. In the case under study $E_{53} \sim 0.35$, and to explain the bump that occurs at $t = t_{\text{shock}} \sim 0.4$ days, the slow material adding energy to the forward shock should have a $\Gamma_{\text{slow},10} = \Gamma_0/10 \sim 2$. In fact, as shown in Sect. 4.3, the average values of Γ_{peak} estimated for the late broad peak of GRB 120326A is of the order of a few tens, and therefore the refreshed-shock scenario could explain the observed behaviour.

A possible drawback of this interpretation is that 1) the peak that we see at late-time is probably not the onset of the forward shock, and therefore the estimate of Γ_{peak} cannot be made accurately; and 2) the observed rising and decaying indices ($\alpha_{\text{BPL,rise}}$ and $\alpha_{\text{BPL,decay}}$ reported in Table 2) in the optical and X-ray bands seem to slightly differ while these values are expected to be consistent in the two bands. However, this can be explained by the different contributions of the early-time emission observed in the two bands. As can be see in Fig. 1, the X-ray emission for $t < 10^3$ s is very steep, and its contribution to the second component would be more relevant for the rising part of the X-ray emission after $\sim 3 \times 10^3$ s, while it would be negligible at very late times. Instead, the early emission is very flat in the optical band and will still contribute at later times, making the light-curve in that band flatter. A marginal difference seems to be present in the observed light-curves at particular frequencies, probably result of the different time coverage (Fig. 1). When considering the rest-frame X-ray and optical luminosities (Fig. 4), however, the agreement between these two bands is straightforward. Despite these small differences, the refreshed-shock scenario cannot be excluded at high confidence level.

The energy-injection scenario has also been analysed in detail for the wind-like and homogeneous circumburst medium by Hou et al. (2014). The authors found that a stellar wind circumburst environment can provide a reasonable fit of the observed X-ray and optical light-curves of GRB 120326A (Hou et al. 2014).

4.6. Density bump

An increase of the external medium density is sometimes invoked to explain the late-time re-brightening in the optical light-curve when a corresponding bump is not seen in the X-ray band

(Lazzati et al. 2002; Dai & Wu 2003). A sharp and large jump in a uniform density profile is needed, however, to produce an observable increase in the observed light-curves. A sudden enhancement by factor $a = 10$ ($\geq 10^2$) of the medium density will correspond to a variation of $\Delta\alpha \leq 0.4$ (≈ 1.0) in the observed temporal slopes. These variations in the temporal decay are only relevant for the radio frequencies. In the optical band, even a strong density enhancement would generate small hard-to-detect variations (Granot et al. 2003; van Eerten et al. 2009). In general, if the observed bump in the optical light-curve for GRB 120326A is produced by the external shock, then any density variation is unlikely to produce the achromatic signature observed in Fig. 1. Therefore, this interpretation seems unlikely.

4.7. Geometrical effect

For a jet with an opening angle θ_{jet} of a few degrees, an observer located at an angle $\theta_{\text{view}} > \theta_{\text{jet}}$ will see a bump in the light-curve at relatively late times when the bulk Lorentz factor of the jet is $1/\Gamma \sim \theta_{\text{view}} - \theta_{\text{jet}}$, because of the jet deceleration (i.e. Granot et al. 2005; Guidorzi et al. 2009). First-order calculations suggest that a jet with a typical opening angle of ~ 3 degrees seen at 5 degrees off-axis could account for the peak. In this scenario, which requires further modelling of the optical and X-ray afterglow light-curve, and whose detailed study is left for a future work, the peak should be achromatic, as observed in GRB 120326A. However, a jet seen off axis cannot account for the relatively high energy of the prompt emission observed in this burst. Even a jet with typical parameters similar to those described above and an isotropic equivalent energy as high as 10^{54} erg could not account for the observed isotropic energy observed since the de-beaming factor would be $\propto \delta^2$.

A possible solution is that a wider jet component or structure (e.g. jet tails) is present, which intercepts the line of sight so as to account for both the prompt emission energy (and peak energy) and the emission observed in the optical before the bump.

4.8. Gravitational microlensing

In principle, achromatic fluctuations in GRB afterglow light-curves, observed less than one day post-burst, might be the result of gravitational microlensing (Loeb & Perna 1998). Such an effect would magnify the observed flux adding a sharp peak on the declining part of the afterglow light-curve for the X-ray and optical (R) band. This explanation was successfully applied to GRB 000301C, a GRB at redshift $z = 2.04$ that displayed an achromatic bump 3.8 days after the burst. That bump corresponded to a flux (magnitude) magnification of ~ 2 (~ 1 mag) in its light-curve (Garnavich et al. 2000).

In the case under study we can estimate the lower limit of flux magnification factor at the peak time $\mu_{\text{obs}}(t_{\text{peak}}) \sim 23.5$ as the ratio between the maximum of the light-curve shown in Fig. 1 and the flux of the early power-law component extrapolated to $t = t_{\text{peak}}$. The estimated factor corresponds to a magnitude magnification of at least 3.4 mag in the afterglow light-curve. Such a strong magnification factor, coupled with the broadness of the observed peak observed, makes this interpretation very unlikely for GRB 120326A.

5. Conclusions

Our multi-band analysis of GRB 120326A allows us to conclude that the striking feature observed in the late-time afterglow light-curve, the broad achromatic re-brightening, cannot be ascribed

to reverse- or forward-shock emission or to the passage of the synchrotron frequency through the optical band. The long duration and magnitude of the re-brightening also make the late flare, the gravitational microlensing, and the density bump origin inconsistent with the observed data.

Although the light-curves are not all fully sampled across all wavebands, we have established that 1) the available data are consistent in the optical/IR bands with an achromatic behaviour, with all light-curves described by the same fitting function rigidly shifted at different wavelengths; 2) the pre-bump (different) emission observed in the X-ray and optical bands is not simply explained with a single emission component, and an additional contribution must be present that shapes the observed light-curves differently after the end of the prompt emission; and 3) the observed late-time behaviour can be explained either by a late-time refreshed forward shock (prolonged energy supply from the central engine) or by a geometrical effect (a two-component jet seen slightly off-axis). We cannot favour one of these two scenarios over the other. A more detailed study of the multi-wavelengths light-curves for a larger sample of events is needed, coupled with good theoretical predictions to compare with well-sampled observations.

References

Barthelmy, S. D., Sakamoto, T., Markwardt, C. B., et al. 2012, GCN Circ., 13120, 1
Bernardini, M. G., Margutti, R., Chincarini, G., et al. 2011, A&A, 526, A27
Beuermann, K., Hessman, F. V., Reinsch, K., et al. 1999, A&A, 352, 26
Burrows, D. N., Falcone, A., Chincarini, G., et al. 2007, RSPTA, 365, 1213
Chincarini, G., Mao, J., Margutti, R., et al. 2010, MNRAS, 406, 2113
Collazzi, A. C. 2012, GCN Circ., 13145, 1
Covino, S., D'Avanzo, P., Klotz, A., et al. 2008, MNRAS, 388, 347
Curran, P., Starling, R. L. C., O'Brien, P. T., et al. 2008, A&A, 487, 533
Dai, Z. G., & Wu, X. F. 2003, ApJ, 591, 21
Dintinjana, B., & Mikuz, B. 2012, GCN Circ., 13113, 1
Filgas, R., Greiner, J., Schady, P., et al. 2012, A&A, 546, A101
Fukugita, M., Shimasaku, K., Ichikawa, T. 1995, PASP, 107, 945
Garnavich, P. M., Loeb, A., & Stanek, K. Z. 2000, ApJ, 544, 11
Gehrels, N., Chincarini, G., Giommi, P., et al. 2004, ApJ, 611, 1005
Genet, F., Daigne, F., & Mochkovitch, R. 2006, AIP Conf., 836, 353
Ghirlanda, G., Nava, L., Ghisellini, G., et al. 2012, MNRAS, 420, 483
Ghisellini, G., Nardini, M., Ghirlanda, G., & Celotti, A. 2009, MNRAS, 393, 253
Granot, J., Nakar, E., & Piran, T. 2003, Nature, 426, 138
Granot, J., Ramirez-Ruiz, E., & Perna, R. 2005, ApJ, 630, 1003
Greiner, J., Krühler, T.; McBreen, S., et al. 2009, ApJ, 693, 1912
Guidorzi, C. 2012, GCN Circ., 13111, 1

Guidorzi, C., Vergani, S. D., Sazonov, S., et al. 2007, A&A, 474, 793
Guidorzi, C., Clemens, C., Kobayashi, S., et al. 2009, A&A, 499, 439
Guidorzi, C., Mundell, C. G., Harrison, R., et al. 2014, MNRAS, 438, 752
Hentunen, V.-P., Nissinen, M., & Salmi, T. 2012, GCN Circ., 13119, 1
Hou, S. J., Geng, J. J., Wang, K., et al. 2014, ApJ, 785, 113
Huang, Y. F., Wu, X. F., Dai, Z. G., Ma, H. T., & Lu, T. 2004, ApJ, 605, 300
Ioka, K., Kobayashi, S., & Zhang, B. 2005, ApJ, 631, 429
Jang, M., Im, M., & Urata, Y. 2012, GCN Circ., 13139, 1
Japelj, J., Kopač, D., Kobayashi, S., et al. 2014, ApJ, 785, 84
Klotz, A., Gendre, B., Boer, M., & Atteia, J. L. 2012a, GCN Circ., 13107, 1
Klotz, A., Gendre, B., Boer, M., & Atteia, J. L. 2012b, GCN Circ., 13108, 1
Kobayashi, S. 2000, ApJ, 545, 807
Kobayashi, S., & Zhang, B. 2003, ApJ, 597, 455
Kopač, D., Kobayashi, S., Gomboc, A., et al. 2013, ApJ, 772, 73
Kuin, N. P. M., Holland, S., & Siegel, M. H. 2012, GCN Circ., 13114, 1
Kumar, P., & Piran, T. 2000, ApJ, 532, 286
Kuroda, D., Hanayama, H., Miyaji, T., et al. 2012a, GCN Circ., 13155, 1
Kuroda, D., Hanayama, H., Miyaji, T., et al. 2012b, GCN Circ., 13170, 1
Kuroda, D., Hanayama, H., Miyaji, T., et al. 2012c, GCN Circ., 13177, 1
La Cluyze, A., Haislip, J., Ivarsen, K., et al. 2012, GCN Circ., 13109, 1
Laskar, T., Zauderer, A., & Berger, E. 2012, GCN Circ., 13181, 1
Lazzati, D., Rossi, E., Covino, S., Ghisellini, G., & Malesani, D. 2002, A&A, 396, 5
Loeb, A., & Perna, R. 1998, ApJ, 495, 597
Margutti, R., Genet, F., Granot, J., et al. 2010, MNRAS, 402, 46
Marshall, Antonelli, L. A., Burrows, D. N., et al. 2011, ApJ, 727, 132
Malandri, A., Mundell, C. G., Kobayashi, S., et al. 2008, ApJ, 686, 1209
Melandri, A., Guidorzi, C., Kobayashi, S., et al. 2009, MNRAS, 395, 1941
Melandri, A., Kobayashi, S., Mundell, C. G., et al. 2010, ApJ, 723, 1331
Melandri, A., Covino, S., Rogantini, D., et al. 2014, A&A, 565, A72
Molinari, E., Vergani, S. D., Malesani, D., et al. 2007, A&A, 469, 13
Monfardini, A., Kobayashi, S., Guidorzi, C., et al. 2006, ApJ, 648, 1125
Morgan, A. N. 2012, GCN Circ., 13143, 1
Mundell, C. G., Melandri, A., Guidorzi, C., et al. 2007, ApJ, 660, 489
Nardini, M., Greiner, J., Krühler, T., et al. 2011a, A&A, 531, A39
Nardini, M., Elliott, J., Filgas, R., et al. 2011b, A&A, 562, A29
Nousek, J. A., Kouveliotou, C., Grupe, D., et al. 2006, ApJ, 642, 389
Panaitescu, A., Mészáros, P., Burrows, D., et al. 2006, MNRAS, 369, 2059
Perley, D. A., Alatalo, K., & Horesh, A. 2012, GCN Circ., 13175, 1
Quadri, U., Strabla, L., Girelli, R., & Quadri, A. 2012a, GCN Circ., 13142, 1
Quadri, U., Strabla, L., Girelli, R., & Quadri, A. 2012b, GCN Circ., 13160, 1
Quadri, U., Strabla, L., Girelli, R., & Quadri, A. 2012c, GCN Circ., 13172, 1
Quadri, U., Strabla, L., Girelli, R., & Quadri, A. 2012d, GCN Circ., 13178, 1
Quadri, U., Strabla, L., Girelli, R., & Quadri, A. 2012e, GCN Circ., 13192, 1
Rees, M. J., & Mészáros, P. 1998, ApJ, 496, 1
Rossi, A., Schulze, S., Klose, S., et al. 2011, A&A, 529, A142
Rykoff, E. S., Aharonian, F., Akerlof, C. W., et al. 2009, ApJ, 702, 489
Schlafly, E. F., & Finkbeiner, D. P. 2011, ApJ, 737, 103
Sari, R., & Mészáros, P. 2000, ApJ, 535, 33
Siegel, M. H., Barthelmy, S. D., Burrows, D. N., et al. 2012, GCN Circ., 13105, 1
Staley, T. D., Titterington, D. J., Fender, R. P., et al. 2012, MNRAS, 428, 3114
Swenson, C. A., Roming, P. W. A., De Pasquale, M., & Oates, S. 2013, ApJ, 774, 2
Tello, J. C., Sanchez-Ramirez, R., Gorosabel, J., et al. 2012, GCN Circ., 13118, 1
Tonincelli, M., Arici, G., Quadri, U., et al. 2012, GCN Circ., 13189, 1
Urata, Y., Huang, K. Y., Takahashi, S., & Petitpas, G. 2012, GCN Circ., 13136, 1
Urata, Y., Huang, K., Takahashi, S., et al. 2014, ApJ, 789, 146
van Eerten, H. J., Meliani, Z., Wijers, R. A. M. J., & Keppens, R. 2009, MNRAS, 398, 63
Virgili, F. J., Mundell, C. G., Pal'shin, V., et al. 2013, ApJ, 778, 54
Walker, C., Court, J., Duffy, R., et al. 2012, GCN Circ., 13112, 1
Zaninoni, E., Bernardini, M. G., Margutti, R., Oates, S., & Chincarini, G. 2013, A&A, 557, A12
Zhao, X.-H., Mao, J., Xu, D., & Bai, J.-M. 2012, GCN Circ., 13122, 1
Zhang, B., Kobayashi, S., & Mészáros, P. 2003, ApJ, 595, 950
Zhang, B., Fan, Y. Z., Dyks, J., et al. 2006, ApJ, 642, 354